Quantifying stochastic noise in cultured circadian reporter cells

Peter C. St. John[1] and Francis J. Doyle III[1,*]

[1]Department of Chemical Engineering, University of California Santa Barbara, Santa Barbara, California 93106-5080
[*]Email: doyle@engineering.ucsb.edu

February 20, 2015

Running head:
Quantifying circadian stochastic noise

Keywords:
Systems Biology | Circadian Rhythms
Gene Regulatory Network | Stochastic | Synchronization

Abstract

Stochastic noise at the cellular level has been shown to play a fundamental role in circadian oscillations, influencing how groups of cells entrain to external cues and perhaps serving as the mechanism by which cell-autonomous rhythms are generated. Despite this importance, few studies have investigated how clock perturbations affect stochastic noise - even as increasing numbers of high-throughput screens categorize how gene knockdowns or small molecules can change clock period and amplitude. This absence is likely due to the difficulty associated with measuring cell-autonomous stochastic noise directly, which requires the careful collection and processing of single-cell data. In this study, we show that since cultured circadian reporters lack significant intercellular coupling, the damping rate of population-level bioluminescence recordings can serve as an accurate measure of cell-autonomous stochastic noise which can be applied to future and existing high-throughput circadian screens. Using cell-autonomous fibroblast data, we first show directly that higher noise at the single-cell results in faster damping at the population level. Next, we show that the damping rate of cultured cells can be changed in a dose-dependent fashion by small molecule modulators, and confirm that such a change can be explained by single-cell noise using a mathematical model. We further demonstrate the insights that can be gained by applying such a method to a genome-wide siRNA screen, revealing that stochastic noise is altered independently from period, amplitude, and phase. Finally, we hypothesize that the unperturbed clock may be highly optimized for robust rhythms, as very few gene perturbations are capable of simultaneously increasing amplitude and lowering stochastic noise. Ultimately, this study demonstrates the importance of considering the effect of circadian perturbations on cell-autonomous noise, especially with regard to the development of small-molecule circadian therapeutics.

Introduction

Circadian rhythms in mammals are daily changes in gene expression and physiology that persist even in the absence of external environmental cues (6). Such rhythms are generated by a large network of interacting regulatory elements, in which time-delayed negative feedback gives rise to sustained oscillations (17). The functional roles of different species in circadian regulation have traditionally been studied using behavioral-level data and genetic knockout experiments (18). Bioluminescence-based cellular circadian reporters offer a more direct view of the gene regulatory network (2), and are amenable to high-throughput screens, allowing genome-wide exploration into factors which affect circadian rhythmicity (21). Additionally, cultured circadian reporter cells allow the change in transcriptional amplitude following a perturbation to be quantified. This additional parameter has proven useful in differentiating between perturbations with the same effect on period (15), and has lead to the search for small-molecule therapeutics which boost clock amplitude (4).

Transcription at the single-cell level is strongly affected by the low molecular counts of the mRNA and protein species involved. As a result, bioluminescence traces of individual cells are stochastic, with significant period-to-period variability (19). The collective behavior of thousands of cells results in more reliable oscillations at the tissue-level, especially in the suprachiasmatic nucleus (SCN) where cell-to-cell coupling keeps individual oscillators at a consistent phase (7). While communication between cells is common in many tissues, it is currently thought that coupling between circadian oscillations outside the SCN, such as in peripheral tissues or cultured reporter cells, is very weak, if present (5, 11). In populations which lack cell-to-cell coupling, stochastic noise at the single-cell level is manifested in damped oscillations at the population-level (19). Despite the averaging which occurs at the population-level, stochastic noise at the single-cell level plays an important role in determining the function of the circadian oscillator. A recent

study showed that stochasticity is critical to the population-level response to a neuropeptide and forms the basis for how the SCN entrains to light-mediated cues (1). Additional studies have even argued that the basis of single-cell rhythmicity depends on stochastic noise, as models of deterministically damped oscillators - when simulated stochastically - better capture the noise characteristics seen in single-cell fibroblast data (20).

Despite the importance of single-cell stochasticity in circadian rhythms, measuring stochastic noise currently requires careful plating and recording of fibroblast cells and subsequent image processing (10). As a result, while circadian perturbations have been postulated to affect single-cell stochasticity (13), no study has experimentally quantified changes to single-cell noise as a result of a small molecule or genetic perturbation. In this study, we demonstrate single-cell stochasticity can be reliably inferred from the damping rate of population-level bioluminescence recordings. Additionally, we show that a small-molecule modulator is able to change circadian noise in a dose-dependent fashion. Finally, we calculate the genome-wide effects of siRNA knock-down on single-cell noise, and demonstrate that population-level damping rate is independent of other circadian parameters, such as period or amplitude. Our results should prove especially important in the future search for small molecule circadian therapeutics, as it allows the effect of candidate drugs on single-cell noise to be quantified in a high-throughput manner.

Materials and Methods

Fitting a damped sinusoid to experimental data

A damped sinusoid, specified by:

$$\hat{y}(t) = Ae^{-dt}\sin\left(\frac{2\pi t}{T} + \theta\right)$$

is fit to experimental data $x_i(t_i)$, $i \in \{0, \ldots, N-1\}$. The x_i data points are first detrended using Hodrick-Prescott filter with a smoothing parameter $\gamma = 0.05\left({}^{24\,\text{hrs}}/_{s}\right)^4$, in which s is the sampling rate (in hours) (12). The detrended data is then filtered using a low-pass filter to remove high-frequency noise (forward-backward Butterworth filter with $n = 5$, $w_c = 0.1$). We denote the detrended and filtered experimental data by $y_i(t_i)$. For numerical efficiency, the period, T, and damping rate, d, parameters are fit first using a matrix pencil method (9), reviewed in (22). Amplitude, A, and phase, θ, parameters are subsequently fit using a linear least-squares regression. Overall R^2 values for the regression were calculated from the residual error between the detrended data and fitted sinusoid:

$$R^2 = 1 - \frac{\sum_{i=0}^{N-1}(y_i(t_i) - \hat{y}(t_i))^2}{\sum_{i=0}^{N-1}(y_i(t_i) - \bar{y}(t_i))^2}$$

Processing single-cell bioluminescence data

Single-cell bioluminescence data for 79 cells was obtained from Leise *et al.*, 2012 (10). As was done in the original study, a discrete wavelet transform (using PyWavelets, `http://www.pybytes.com/pywavelets`) was performed to detrend and remove noise.

Sorting cells by noise level

As in the original study, various parameters describing the average noise level of each cell were collected. Traces were denoised and detrended by keeping only the $(8\text{hr}, 258\text{hr})$ wavelet com-

ponents. From these smoothed trajectories, a Hilbert transform was used estimate points at which the phase crossed 0 to find period and amplitude coefficients of variation. An additional noise parameter, the standard deviation in the $(1\text{hr}, 8\text{hr})$ wavelet components divided by the overall rhythm amplitude, was used to quantify the high-frequency noise of the system. From these three noise variables, a combined noise metric was constructed by projecting the variables along their first principle component (using scikit-learn, `http://scikit-learn.org/`). Cells were ranked according to this combined noise metric, and a high-noise group and low-noise group were constructed by taking the 39 highest-noise and lowest-noise cells, respectively. The raw bioluminescence profiles were not initially synchronized, so in order to simulate the gradual desynchronization of a group of oscillators the traces were offset to have the same starting phase. This was accomplished by starting each trace at the first phase zero-crossing, which were found using a Hilbert transform.

Bootstrap estimations of the damping rate difference

Averaged traces for low and high-noise group displayed a damped sinusoidal rhythm. The first 4 days of rhythms ($s = 0.5,\ N = 192$) were fit using a damped sinusoid. To ensure the difference in damping rate between groups was statistically significant, a bootstrap analysis was performed. In each of $10,000$ bootstrap trials, the cells were randomly assigned evenly to either the low-noise or the high-noise group. The absolute difference in damping rate between the two populations was recorded to yield a two-tailed test. The observed test statistic, $|d_h - d_l| = 6.65 \times 10^{-3}$, was found to be significant at the $\alpha = 0.05$ confidence threshold ($p = 0.0264$).

Quantifying dose-dependent effects of small molecule modulators

Bioluminescence traces ($s = 1.67,\ N = 71$) from the application of increasing concentrations of small molecule were fit using the method described in a previous section. Because the small molecules were toxic to the cells at very high concentrations, experiments were removed from further analysis when the R^2 of the sinusoidal regression fell below 0.80 (Figure S1).

In silico prediction of small molecule experiments

A previously published mathematical model of circadian rhythms was used to predict the effects on population damping rate from the dose-dependent small molecule experiments (8). The parameters used to capture the effects of each small molecule were the same as described previously (15). The model was converted to a stochastic biochemical system and subsequently simulated using StochKit2 (14). Population-level rhythms were found by taking the average of $1,000$ noninteracting oscillators, starting at identical initial conditions. The only parameter left unspecified by the deterministic model was the cell volume Ω, which controlled the amount of noise in the system. For a given Ω, the population-level damping rate was found by finding the phase diffusivity parameter which gave the closest fit to the simulated population-level rhythms, as described in (16). An R^2 value was calculated for each fit, taking into account all eight state variables.

Fitting the volume parameter

We calculated an average experimental damping rate of $d = 0.0151$ from the $0\mu M$ bioluminescence trajectories for both KL001 and longdaysin. *In silico* damping rates were calculated for

logarithmically space values of $\Omega \in (100, 500)$. Ten independent groups of $1,000$ oscillators were simulated for each Ω, from which the means and standard errors were found. Simulations in which $R^2 < 0.90$ were removed from further analysis. A weighted least-squares regression (using statsmodels, `http://statsmodels.sourceforge.net/`) was performed for $\log d$ vs. $\log \Omega$, using the $\log \mathrm{SEM}$ of each measurement as a regression weight (Figure S2). The best fit was found to be $\Omega = 226.3 \pm 9.0$.

Parameter knockdown experiments

We mathematically replicated the effects of the small molecules KL001 and longdaysin through the reductions of the *vdcn* and *vac*1*p* parameters, respectively. Simulations were performed with 20 values of each parameter, linearly spaced between 100% and 15% of their nominal value. Similar to the volume calibration simulations, 10 independent groups of $1,000$ oscillators were simulated from an initially entrained state. Means and standard errors in period and damping rate were calculated from each trajectory. Simulations in which $R^2 < 0.90$ were removed from further analysis.

Fitting the genome-wide siRNA screen

We analyzed the supplemental annotations and data for the $111,743$ wells ($s = 2,\ N = 72$) in the Zhang *et al.*, 2009 screen (21). Fits for which the $R^2 < 0.80$ were discarded. We rescaled amplitude values on a logarithmic basis, as these were more normally distributed. Plate to plate variation, as shown in Figure S3, was more severe than variation on a well-to-well basis, Figure S4. Parameters were therefore normalized on a plate-by-plate basis using a robust z-score (3):

$$z_{R,i} = \frac{x_i - M(x_i)}{M\left(|x_i - M(x_i)|\right)}, \qquad i \in \{0, \ldots, \mathcal{P} - 1\}$$

where $M(\cdot)$ denotes the median of a vector, and x_i contains all the points in one plate, and $\mathcal{P}$ is the number of plates. We removed outlier points prior to calculating the moments of the distributions, Pearson correlation coefficients, and performing the multivariable linear regression. Outliers were defined as points which contained any z-metric with an absolute value greater than eight. We chose the "control" wells to be those which contained no siRNA, as these proved to be more numerous than those containing reference siRNA perturbations and were clustered similarly to the highest-density regions of the perturbed fits.

Detecting outlier perturbations

We found the average perturbed response by grouping the perturbed dataset by target gene ID (using pandas, `http://pandas.pydata.org/`). A Hotelling's T^2 test was used to determine whether the means of each gene knockdown was significantly different from the control population. A robust covariance estimator was used to find the location and covariance of the control distribution (using scikit-learn). Because the control distribution ($n = 11,253$) is much larger than that for any particular gene ID ($n \approx 4$), we assume the combined covariance is equal to the covariance of the control sample alone.

Results and Discussion

Single-cell stochastic noise is manifested in damped population-level rhythms

We first sought to determine whether single-cell stochastic noise affects the population-level damping rate in cultured bioluminescence cells. To do this, we calculated noise characteristics from experimental data on individual PER2::LUC fibroblast cells (10). We sorted the cells into two groups, a low-noise group and a high-noise group, based on the relative high-frequency noise, period variability, and amplitude variability present in each trace. Example rhythms from cells in both groups are shown in Figure 1A. Because the cells were not synchronized at the start of the recording, we replicate this effect *in silico* by shifting each series in time to align their start phases. We next calculated expected population-level bioluminescence traces by averaging the cellular PER2::LUC signal in each group. Both populations displayed averaged rhythms which resembled a damped sinusoid, similar to those seen in bioluminescence recordings of entire cell cultures . Fitting the averaged expression of each group with a damped sinusoid revealed that the low-noise group also had a lower damping rate (Figure 1B). The significance of this difference was confirmed via a bootstrap analysis (Figure 1C), where in each bootstrap trial cells were randomly assigned to either the low-noise or the high-noise group.

Clock perturbations can change single-cell stochastic noise

We next demonstrate that perturbations to the transcriptional oscillator are capable of altering single-cell level stochastic noise. The actions small-molecule circadian modulators KL001 and longdaysin are well-characterized, and are known to affect circadian period and amplitude in a dose-dependent fashion (15). By fitting experimental data on the population-level responses to increasing dosages of each molecule with a damped sinusoid, we show that KL001, but not longdaysin, increases damping rate in a dose-dependent fashion (Figure 2). This change in damping rate is consistent across both reporter systems (*Bmal1-dLuc* and *Per2-dLuc*), indicating it is a fundamental property of the overall gene regulatory network.

To lend further support to the conclusion that the dose-dependent change in damping rate from KL001 is due to changes in single-cell noise characteristics, we employed a model of circadian rhythms previously used to explain the effects of both small molecule perturbations (15). In order to capture changes to noise characteristics, the model had to first be converted to a stochastic biochemical system. Population-level rhythms were therefore generated by averaging the rhythms of $1,000$ individual, noninteracting oscillators. The only free parameter in converting the existing deterministic model to a stochastic one is the cell volume, which was determined by fitting the observed population-level damping rate to the experimental unperturbed controls (Figure S2).

The model was then used to predict the effects of KL001 and longdaysin administration on single-cell noise and population damping rates (Figure 3A). Reductions in parameters previously attributed to the activities of each small molecule caused dose dependent changes in period and damping rate at the population-level which closely matched experimental results (Figure 3B). As the model includes no cell to cell communication, this difference is manifested solely by changing the noise characteristics of individual cells.

Genome-wide effects of siRNA knockdown on single-cell stochastic noise

Unlike from using single-cell imaging, inferring stochastic noise from the desynchronization rate of population-level recordings can be applied to existing and future high-throughput circadian

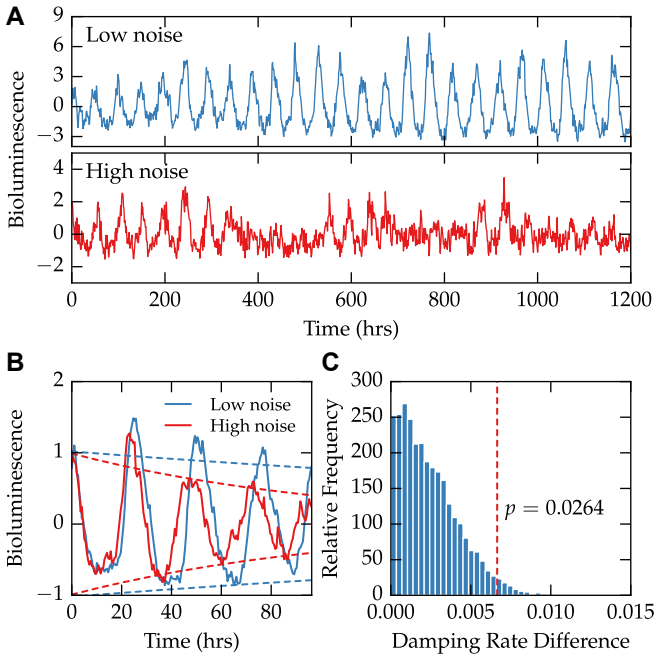

Figure 1: Single-cell bioluminescence recordings show that higher stochastic noise results in faster damping at the population-level. Data on the bioluminescence of single-cell fibroblasts was taken from Leise *et al.*, 2012 (10). (**A**) Cells were sorted into two groups depending on their degree of stochastic noise. An example trace from each of the two groups is shown, demonstrating different levels of noise present in the dataset. (**B**) After artificially synchronizing each cell, averaged bioluminescence rhythms of each group (solid lines) resemble damped recordings taken at cell culture level. A damped sinusoid fit to both both groups reveals a difference in damping rate, demonstrated by fitted envelope functions ($\pm A \exp -dt$, dashed lines). (**C**) The observed absolute difference in damping rate was shown to be significant ($p = 0.0264$) using $10,000$ bootstrap trials.

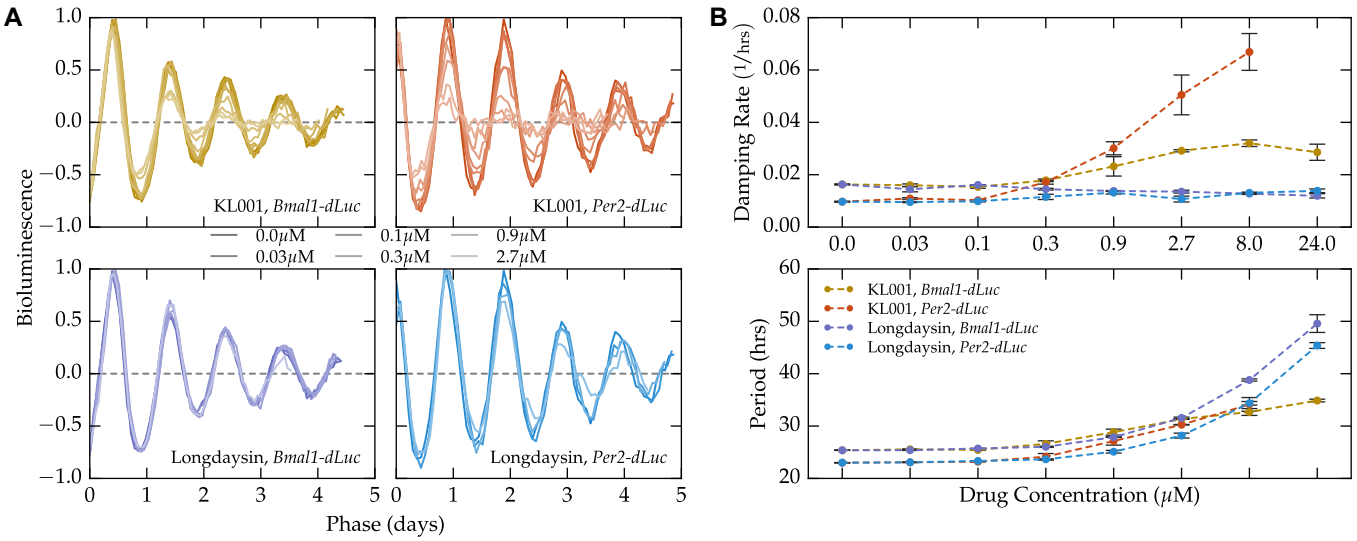

Figure 2: Small molecule modulator KL001 increases damping rate in a dose-dependent fashion. Experimental data on the dose-dependent effect of small molecules KL001 and Longdaysin on cultured circadian reporter cells was taken from Hirota *et al.*, 2012 (8). (**A**) Detrended bioluminescence signals from the two cells and two reporter systems, normalized by the fitted amplitude, period, and phase. The normalized bioluminescence highlights the dose-dependent change in damping rate seen with the KL001 application, but not with longdaysin. (**B**) Quantification of the dose-dependent change in damping rate caused by small molecule modulators. While both molecules lead to a dose-dependent increase in period, only KL001 shows a reliable change in damping rate.

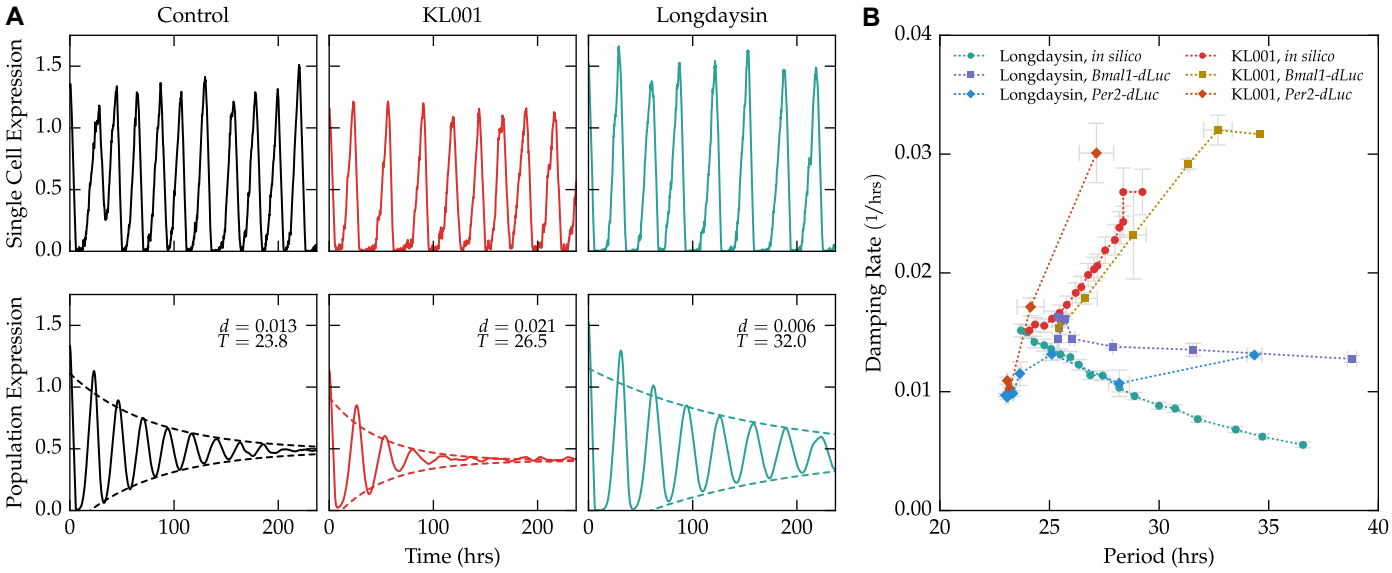

Figure 3: Mathematical model accurately predicts dose-dependent changes in damping rate. (**A**) Example single-cell trajectories (top) and population-averaged trajectories (mean of 1,000 cells, bottom) of cells under various treatments. Cells with the nominal parameter set (left, black) closely match the experimental damping rate for unperturbed cells. Cells with simulated KL001 action (red, center) are noisier at the single-cell level, and show faster damping at the population-level. Cells with simulated longdaysin action show slightly more accurate single-cell rhythms, with a corresponding dip in the population-level damping rate. (**B**) The model accurately predicts the general trend of period vs. damping rate for both KL001 and longdaysin perturbations. Experimental data points represent the mean of two replications at each concentration. Computational data points represent the mean of ten independent population simulations.

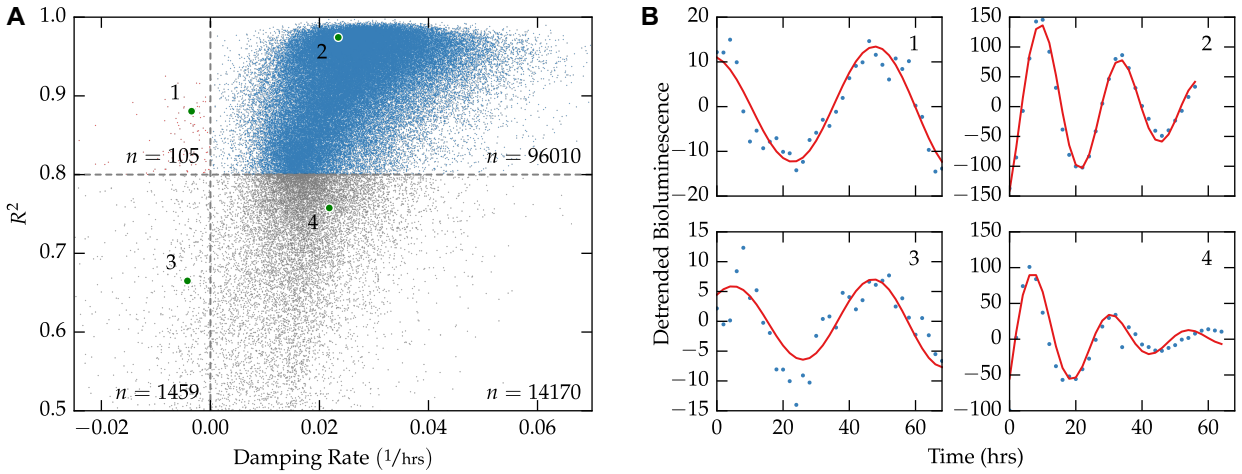

Figure 4: Fit quality vs. damping rate for the genome-wide siRNA screen. (**A**) A plot of the 111,743 individual fits shows that the majority of fits have a high R^2 value and positive damping rate. Only fits with $R^2 > 0.8$ were kept for further analysis. (**B**) Examples chosen randomly from each of the four quadrant regions in (A). Sinusoidal parameters for fits 1-2 can be more confidently inferred than those for fits 3-4.

screens. We demonstrate the insights that can be gained from such an approach by analyzing the publicly available genome-wide siRNA screen from Zhang *et al.*, 2009 (21). The results of fitting a damped sinusoid to each of the 111,743 bioluminescence trajectories is shown in Figure 4, in which 86% of fits had an $R^2 > 0.8$. Since sinusoidal parameters can only be confidently inferred for fits in which the R^2 was sufficiently high, wells were removed from further analysis if $R^2 < 0.8$. Additionally, of the fits with a high R^2 value, only a small minority had a negative damping rate (0.1%): lending further support to the assumption that intercellular synchronization is unlikely in cultured U2OS cells.

We next checked variation of the parameters on a plate-to-plate and well-to-well basis. Well-to-well variation was relatively absent, aside from expected variation due to long- and short-period controls (Figure S4). Fits were normalized to remove plate-to-plate variation (Figure S3) using a robust z-score (3). Additionally, we separated wells into a "perturbed" category and "control" category, depending on whether or not the well contained an siRNA perturbation. As we show in Figure 5, all fitted parameters displayed normal-like distributions, in which the control distributions showed much tighter clustering around the most likely values. Quantifications of the mean, variance, skew, and kurtosis for each distribution are shown in Table 1.

Damping rate is independent of other sinusoidal parameters

Since an siRNA's effect on period length does not effectively predict its effect on amplitude or phase (and vice-versa), we hypothesized that stochastic noise would similarly be independently affected by siRNA perturbations. Low Pearson correlation coefficients between normalized parameter distributions defend this hypothesis, with the highest correlations among variables seen between amplitude and damping rate ($\rho = 0.285$, Table 2). Additionally, a multivariate linear regression of damping rate as a function of period, amplitude, phase, and perturbation type (control or perturbed, a categorical variable) produced an R^2 value of only 0.169 (Table S1).

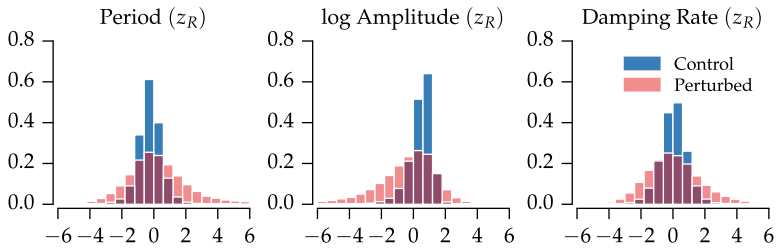

Figure 5: Distributions in fitted parameters for the genome-wide siRNA screen. Distributions in normalized parameter values closely resemble Gaussian distributions. For all parameters, the region of highest density is consistent between the control and perturbed populations, indicating many perturbations do not appreciably change clock dynamics.

	T		$\ln A$		d	
	C	P	C	P	C	P
μ	−0.234	0.187	0.443	−0.343	0.043	0.090
σ	0.774	1.820	0.778	1.753	0.878	1.688
Skew	0.153	0.367	-1.823	−0.580	-0.107	0.371
Kurt	3.772	0.591	8.329	0.476	2.423	0.373

Table 1: Moments of the fitted parameter distributions (Figure 5) after normalization and outlier removal. Parameters were normalized by subtracting the median and dividing by the median absolute deviation on a plate-by-plate basis. Control distributions were less skewed and more peaked then their perturbed counterparts.

	d	$\ln A$	T	θ
d	1.000	0.285	−0.142	−0.269
$\ln A$	0.285	1.000	−0.022	−0.112
T	−0.142	−0.022	1.000	−0.113
θ	−0.269	−0.112	−0.113	1.000

Table 2: Correlation among normalized parameters of the high-throughput siRNA screen. Pearson correlation coefficients are relatively low between fitted parameters, indicating that changes to damping rate (and thereby stochastic noise) are not explained by changes to period, amplitude, or phase.

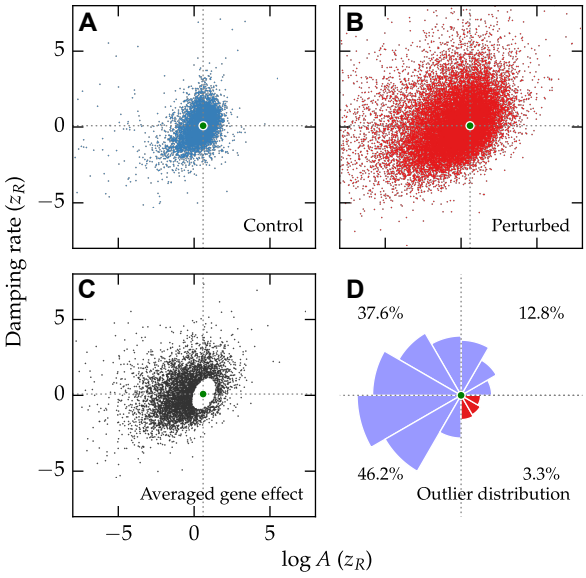

Figure 6: Effects of siRNA knockdowns on amplitude and damping rate. Clock robustness is a function of both amplitude and damping rate. Distributions in amplitude and damping rate for control wells (**A**) or perturbed wells (**B**) indicate that perturbations tend to shift the clock towards regions of higher damping rate or lower amplitude. Green dots in each figure indicates the mean of the control population. (**C**) Averaged effect of siRNA knockdown after grouping the perturbed population by Gene ID. Only those genes which were significantly different from the control distribution are shown (Hotelling's T^2 test, $\alpha = 0.01$). (**D**) Radial histogram of the significant gene perturbations shown in (C). The area of each slice is proportional to the frequency of perturbations away from the mean in that direction. Very few gene knockdowns resulting in both higher amplitude and lower damping rate (red slices, lower right quadrant).

The unperturbed clock may lie at the Pareto frontier of high amplitude and low noise

The ability of a population of oscillators to maintain robust oscillations is a function both of its initial amplitude as well as its damping rate. A robust oscillator is therefore one with high amplitude and low stochastic noise. Scatter plots of the control and perturbed distributions are shown in Figure 6A-B, which indicate perturbations tend to shift the clock towards less robust regions of oscillations. In order to find perturbations which confidently change robustness, we grouped the siRNA perturbations by target gene and performed a two-sample Hotelling's T^2 test against the control population. The resulting significant gene perturbations (75% of all genes) are shown in Figure 6C. Quantifying the distribution in outliers by quadrant, it is clear that only a small minority of perturbations, 3.3%, simultaneously increase amplitude and decrease stochastic noise. It therefore appears that the unperturbed clock optimizes some trade-off between oscillator amplitude and stochastic noise, such that it is not feasible to make oscillations more robust by knocking down one gene at a time.

Conclusion

In this study, we have described a method by which stochastic noise can be estimated from population-level bioluminescence recordings. As high amplitude circadian oscillations are important for maintaining metabolic health, many studies have sought to find small molecule candidates which increase oscillatory amplitude (4). In the search for circadian clock therapeutics, high-throughput methods are frequently used to screen for such drugs, often neglecting potential effects on cell-autonomous noise. While we have demonstrated a method by which the effects of small molecules on noise can be inferred from high-throughput methods, we have also shown that the potential improvement of clock robustness may be limited. Amplitudes of circadian rhythms may be best bolstered by small molecule therapies by finding drugs which act transiently to synchronize peripheral oscillators. While such a method would require accurate alignment of drug administration to the correct circadian phase, a recent *in silico* study has demonstrated the potential effectiveness of such an approach in improving amplitudes in peripheral tissues (16).

Acknowledgments

This work was supported by the National Institutes of Health/National Institute of General Medical Sciences under award number 1R01GM096873-01 and by the Institute for Collaborative Biotechnologies through grant W911NF-09-0001 from the U.S. Army Research Office.

References

1. An S, Harang R, Meeker K, Granados-Fuentes D, Tsai Ca, Mazuski C, Kim J, Doyle FJ, Petzold LR, Herzog ED (2013) A neuropeptide speeds circadian entrainment by reducing intercellular synchrony. *Proc Natl Acad Sci U S A* **110**: E4355–61

2. Balsalobre A, Damiola F, Schibler U (1998) A serum shock induces circadian gene expression in mammalian tissue culture cells. *Cell* **93**: 929–37

3. Birmingham A, Selfors LM, Forster T, Wrobel D, Kennedy CJ, Shanks E, Santoyo-Lopez J, Dunican DJ, Long A, Kelleher D, Smith Q, Beijersbergen RL, Ghazal P, Shamu CE (2009) Statistical methods for analysis of high-throughput RNA interference screens. *Nat Methods* **6**: 569–75

4. Chen Z, Yoo SH, Takahashi JS (2013) Small molecule modifiers of circadian clocks. *Cell Mol Life Sci* **70**: 2985–98

5. Guenthner CJ, Luitje ME, Pyle La, Molyneux PC, Yu JK, Li AS, Leise TL, Harrington ME (2014) Circadian rhythms of Per2::Luc in individual primary mouse hepatocytes and cultures. *PLoS One* **9**: e87573

6. Herzog ED (2007) Neurons and networks in daily rhythms. *Nat Rev Neurosci* **8**: 790–802

7. Herzog ED, Aton SJ, Numano R, Sakaki Y, Tei H (2004) Temporal precision in the mammalian circadian system: a reliable clock from less reliable neurons. *J Biol Rhythms* **19**: 35–46

8. Hirota T, Lee JW, St. John PC, Sawa M, Iwaisako K, Noguchi T, Pongsawakul PY, Sonntag T, Welsh DK, Brenner DA, Doyle FJ, Schultz PG, Kay SA (2012) Identification of Small Molecule Activators of Cryptochrome. *Science* **337**: 1094–1097

9. Hua Y, Sarkar T (1990) Matrix pencil method for estimating parameters of exponentially damped/undamped sinusoids in noise. *IEEE Trans Acoust* **38**: 814–824

10. Leise TL, Wang CW, Gitis PJ, Welsh DK (2012) Persistent cell-autonomous circadian oscillations in fibroblasts revealed by six-week single-cell imaging of PER2::LUC bioluminescence. *PLoS One* **7**: 1–10

11. Noguchi T, Wang LL, Welsh DK (2013) Fibroblast PER2 circadian rhythmicity depends on cell density. *J Biol Rhythms* **28**: 183–92

12. Ravn M, Uhlig H (2002) On adjusting the Hodrick-Prescott Filter for the frequency of observations **84**

13. Rougemont J, Naef F (2007) Dynamical signatures of cellular fluctuations and oscillator stability in peripheral circadian clocks. *Mol Syst Biol* **3**: 93

14. Sanft KR, Wu S, Roh M, Fu J, Lim RK, Petzold LR (2011) StochKit2: software for discrete stochastic simulation of biochemical systems with events. *Bioinformatics* **27**: 2457–8

15. St. John PC, Hirota T, Kay SA, Doyle FJ (2014) Spatiotemporal separation of PER and CRY posttranslational regulation in the mammalian circadian clock. *Proc Natl Acad Sci U S A* **111**: 2040–5

16. St. John PC, Taylor SR, Abel JH, Doyle FJ (2014) Amplitude Metrics for Cellular Circadian Bioluminescence Reporters. *Biophys J* **107**: 2712–2722

17. Ueda HR, Hayashi S, Chen W, Sano M, Machida M, Shigeyoshi Y, Iino M, Hashimoto S (2005) System-level identification of transcriptional circuits underlying mammalian circadian clocks. *Nat Genet* **37**: 187–92

18. Vitaterna MH, King DP, Chang aM, Kornhauser JM, Lowrey PL, McDonald JD, Dove WF, Pinto LH, Turek FW, Takahashi JS (1994) Mutagenesis and mapping of a mouse gene, Clock, essential for circadian behavior. *Science* **264**: 719–725

19. Welsh DK, Yoo SH, Liu AC, Takahashi JS, Kay SA (2004) Bioluminescence imaging of individual fibroblasts reveals persistent, independently phased circadian rhythms of clock gene expression. *Curr Biol* **14**: 2289–95

20. Westermark PlO, Welsh DK, Okamura H, Herzel H (2009) Quantification of circadian rhythms in single cells. *PLoS Comput Biol* **5**: e1000580

21. Zhang EE, Liu AC, Hirota T, Miraglia LJ, Welch G, Pongsawakul PY, Liu X, Atwood A, Huss JW, Janes J, Su AI, Hogenesch JB, Kay SA (2009) A genome-wide RNAi screen for modifiers of the circadian clock in human cells. *Cell* **139**: 199–210

22. ZieliÅĎski TP, Duda K (2011) Frequency and damping estimation methods - An overview. *Metrol Meas Syst* **18**: 505–528

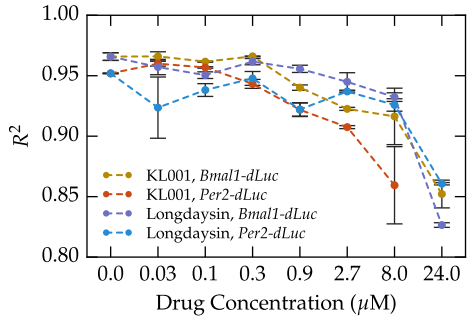

Figure S1: Fit quality for the dose-dependent small molecule screens. The bioluminescence rhythms in both reporter systems were well-described by a damped sinusoid. As the molecules were toxic to the reporter cells at high concentrations, fit quality declined with increasing dosage. Only fits with $R^2 > 0.8$ were kept for further analysis.

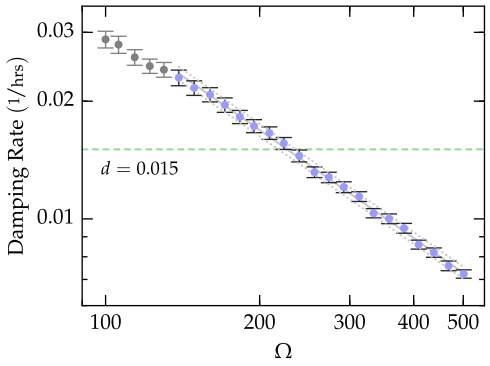

Figure S2: Calibration curve for fitting the volume parameter to experimental data. The model's volume parameter was linearly related to the population-averaged damping rate on a log-log scale. Error bars represent the standard error of the mean, calculated by 10 independent replicates for each volume. Points shown in gray had an average $R^2 < 0.9$ and were excluded from the linear regression. Solid and dashed grey lines indicate the mean and 95% confidence intervals of the linear regression, respectively.

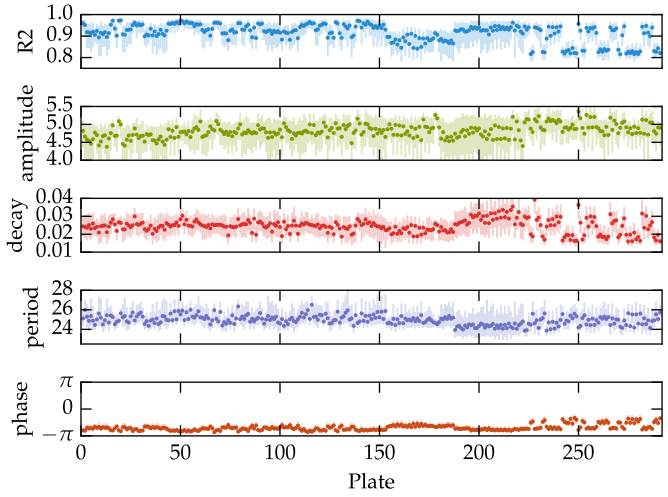

Figure S3: Plate-to-plate variation of fitted parameters in the Zhang *et al.*, 2009 genome-wide siRNA screen. Dots indicate the median of each plate, with lines extending from the 5th to 95th percentile. While parameter fits were largely consistent between plates, some plates had definitively different value ranges. In order to accurately compare perturbations and controls between plate experiments, we normalized fitted parameters on a plate-by-plate basis.

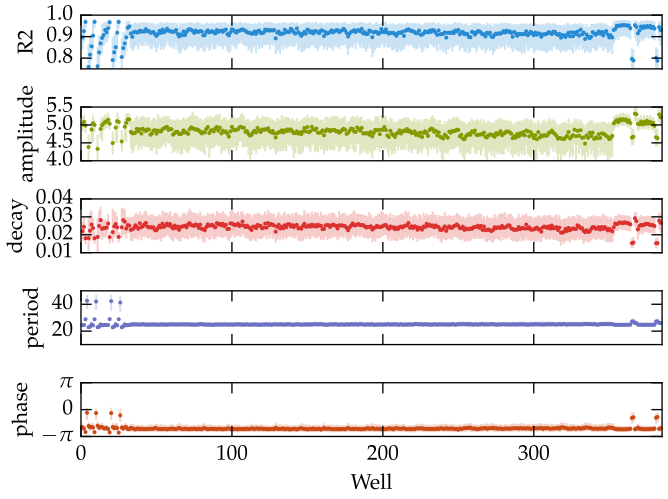

Figure S4: Well-to-well variation in the Zhang *et al.*, 2009 genome-wide siRNA screen. Similar to Figure S3, dots indicate the median value of each parameter in each well, with lines extending from the 5th to 95th percentile. Well position did not seem to affect the fitted values, particularly in the middle regions which contained the siRNA knockdown library. Wells on either end showed significant variation, but these are likely due to the spotting of long- and short-period controls in the same position on each plate.

Dep. Variable:	Damping Rate	**R-squared:**	0.169
Model:	OLS	**Adj. R-squared:**	0.169
Method:	Least Squares	**F-statistic:**	4782.
Date:	Wed, 11 Feb 2015	**Prob (F-statistic):**	0.00
Time:	16:26:22	**Log-Likelihood:**	$-1.7248e+05$
No. Observations:	94053	**AIC:**	$3.450e+05$
Df Residuals:	94048	**BIC:**	$3.450e+05$

	coef	**std err**	**t**	**P>|t|**	**[95.0% Conf. Int.]**
intercept	-0.0370	0.014	-2.572	0.010	$-0.065, -0.009$
amplitude	0.2375	0.003	86.282	0.000	$0.232, 0.243$
period	-0.1521	0.003	56.798	0.000	$-0.157, -0.147$
phase	-0.2354	0.003	85.598	0.000	$-0.241, -0.230$
perturbation type	0.3197	0.015	20.664	0.000	$0.289, 0.350$

Omnibus:	9769.391	**Durbin-Watson:**	1.876
Prob(Omnibus):	0.000	**Jarque-Bera (JB):**	18459.719
Skew:	0.697	**Prob(JB):**	0.00
Kurtosis:	4.664	**Cond. No.**	8.34

Table S1: Multivariable linear regression results. Fit statistics which demonstrate the effect of each other fitted parameter on damping rate. Of particular note is the perturbation type categorical variable, which demonstrates that the presence of siRNA perturbation increases damping rate on average. Higher amplitude is also correlated with higher damping rate. However, in total damping rate is poorly predicted by the other fitted variables $R^2 = 0.169$, indicating it describes an independent oscillatory feature.